

NEUROIMAGING

The PET tracer [¹¹C]MK-6884 quantifies M4 muscarinic receptor in rhesus monkeys and patients with Alzheimer's disease

Wenping Li^{1*}, Yuchuan Wang¹, Talakad G. Lohith¹, Zhizhen Zeng¹, Ling Tong¹, Robert Mazzola¹, Kerry Riffel¹, Patricia Miller¹, Mona Purcell¹, Marie Holahan¹, Hyking Haley¹, Liza Gantert¹, David Hesk¹, Sumei Ren¹, John Morrow¹, Jason Uslaner¹, Arie Struyk¹, Jenny Miu-Chun Wai¹, Michael T. Rudd¹, David M. Tellers¹, Thomas McAvoy¹, Guy Bormans², Michel Koole³, Koen Van Laere³, Kim Serdons³, Jan de Hoon⁴, Ruben Declercq⁵, Inge De Lepeleire⁵, Maria B. Pascual^{6,7}, Paolo Zanotti-Fregonara^{6,7}, Meixiang Yu^{6,7}, Victoria Arbones⁶, Joseph C. Masdeu^{6,7}, Amy Cheng¹, Azher Hussain¹, Tjerk Bueters¹, Matt S. Anderson¹, Eric D. Hostetler¹, Anthony S. Basile¹

Positron emission tomography (PET) ligands play an important role in the development of therapeutics by serving as target engagement or pharmacodynamic biomarkers. Here, we describe the discovery and translation of the PET tracer [¹¹C]MK-6884 from rhesus monkeys to patients with Alzheimer's disease (AD). [³H]MK-6884/[¹¹C]MK-6884 binds with high binding affinity and good selectivity to an allosteric site on M4 muscarinic cholinergic receptors (M4Rs) in vitro and shows a regional distribution in the brain consistent with M4R localization in vivo. The tracer demonstrates target engagement of positive allosteric modulators of the M4R (M4 PAMs) through competitive binding interactions. [¹¹C]MK-6884 binding is enhanced in vitro by the orthosteric M4R agonist carbachol and indirectly in vivo by the acetylcholinesterase inhibitor donepezil in rhesus monkeys and healthy volunteers, consistent with its pharmacology as a highly cooperative M4 PAM. PET imaging of [¹¹C]MK-6884 in patients with AD identified substantial regional differences quantified as nondisplaceable binding potential (BP_{ND}) of [¹¹C]MK-6884. These results suggest that [¹¹C]MK-6884 is a useful target engagement biomarker for M4 PAMs but may also act as a sensitive probe of neuropathological changes in the brains of patients with AD.

INTRODUCTION

Alzheimer's disease (AD) is a progressive neurodegenerative disease not only characterized primarily by cognitive deficits but also associated with a heterogeneous array of aberrant behaviors including physical aggression, screaming, suspiciousness, hallucinations, and delusions, collectively termed neuropsychiatric symptoms (NPSs) of dementia (1). NPSs are manifested by up to 97% of patients with AD at some point during the disease (2). Although some of the symptoms of NPS are currently treated with antipsychotics such as risperidone, these agents are of modest efficacy and have substantial adverse effects, including increased risk of falls and sudden death (3).

Given the unmet medical need for treatments of NPS, the M1/M4 muscarinic acetylcholinergic receptor (mAChR) orthosteric agonist xanomeline was tested in patients with AD and found to effectively enhance cognitive function and reduce the incidence of delusions, hallucinations, and suspiciousness (4, 5). Subsequent investigations support the claim that the clinical effects of xanomeline are mediated primarily by the M4 subtype of muscarinic acetylcholine (ACh) receptors (M4Rs) (6). M4Rs have long been viewed as a viable therapeutic target for treating schizophrenia and AD (6, 7) based on their

expression in key brain regions, including the cortex, striatum, and hippocampus (8), as well as from mechanistic (7, 9, 10) and behavioral studies (11, 12). However, targeting the M4R requires high ligand selectivity to avoid the adverse events arising from activation of off-target mAChR subtypes, as observed with xanomeline (13). This lack of selectivity for the M4R subtype is intrinsic to the pharmacology of xanomeline as an orthosteric agonist, given that the coding for the amino acid sequence of the orthosteric binding site for ACh is highly conserved between mAChR receptor subtypes (14, 15). This reduces the probability of developing a ligand that is highly selective for the M4R. An alternative approach for enhancing selectivity is to develop agents targeting allosteric modulatory sites on these receptors, for which the sequences are less homologous across receptor subtypes, if not unique.

Assessment of target engagement is one of the fundamental components of early-stage drug development in neuroscience (16), with positron emission tomography (PET) imaging of drug-target interactions in the brain serving as an important tool (17). To develop a specific PET tracer for measuring target engagement and to facilitate the development of an M4 selective positive allosteric modulator (M4 PAM) for the treatment of NPS, the PET tracer would itself need to selectively bind the same M4R allosteric modulatory site as the therapeutic candidate. Moreover, the extensive loss of cholinergic pathways (18) and accompanying changes in muscarinic receptor expression reported in AD (19–21) suggests that patients may not respond to treatment with an M4 PAM if the endogenous agonist or target receptor is no longer present in relevant brain regions. Given that many of the manifestations of NPS resemble an overactivation

¹MRL, Merck & Co. Inc., Kenilworth, NJ 07033, USA. ²Laboratory for Radiopharmaceutical Research, KU Leuven, 3001 Leuven, Belgium. ³Nuclear Medicine and Molecular Imaging, KU Leuven and University Hospital Leuven, 3001 Leuven, Belgium. ⁴Center for Clinical Pharmacology, KU Leuven, 3001 Leuven, Belgium. ⁵Translational Pharmacology Europe, MSD (Europe) Inc., 1200 Brussels, Belgium. ⁶Nantz National Alzheimer Center, Houston Methodist Neurological Institute, Houston, TX 77030, USA. ⁷Department of Neurology, Weill Cornell Medicine, New York, NY 10065, USA.

*Corresponding author. Email: wenping_li@merck.com

of dopaminergic pathways (9, 22), it is important that the striatal M4R populations regulating dopaminergic neurotransmission remain intact. Currently, there remains uncertainty over the regional status of M4R in brain regions (particularly striatum) of patients with AD, primarily due to a lack of specificity of the orthosteric muscarinic ligands used for both in vitro and in vivo investigations (20, 23, 24). Therefore, a PET tracer that binds to an allosteric modulatory site may provide not only information about target selectivity and receptor occupancy (RO) but also evidence of a cooperative interaction with the orthosteric site such that the presence of the endogenous ligand should reciprocally influence the binding of the allosteric modulator.

We recently reported the discovery of [^{11}C]MK-6884, an M4 PAM with high binding affinity [inhibition constant (K_i) = 0.19 nM], high cooperativity with the orthosteric site (α = 43), moderate lipophilicity (shake-flask LogD = 2.7), good central nervous system permeability (P_{app} = 28.8×10^{-6} cm/s), and low susceptibility for human P-glycoprotein transport (BA/AB ratio = 0.7) (25). We now provide a more detailed characterization and validation of this selective M4 PAM PET tracer, [^{11}C]MK-6884, for determining the pharmacology and density of M4R in human brain of patients with AD and healthy individuals. [^{11}C]MK-6884 may not only serve as a tool for evaluating target engagement in the development of therapeutics directed at the M4R (25) but also provide insights into the status of cholinergic pathways affected by the neuropathology underlying AD.

RESULTS

Radiochemistry

[^{11}C]MK-6884 was synthesized under good manufacturing practice conditions with high radiochemical purity (>95%) and molar activity (39 to 741 GBq/ μmol) by alkylation of the corresponding lactam with [^{11}C]methyl iodide (Fig. 1A). The final preparation for injection consists of $\leq 4.9 \mu\text{g}$ of [^{11}C]MK-6884 in a sterile solution of up to 10% (v/v) ethanol and 10 mM sodium phosphate buffer (pH 7) in 0.9% sodium chloride. [^3H]MK-6884 was prepared with high molar activity (2.0 GBq/ μmol) and high radiochemical purity (99.9%) by

catalytic tritium dehalogenation of the corresponding bis-iodoaryl precursor (Fig. 1B).

Characterization of [^3H]MK-6884 binding to brain tissues in vitro

Autoradiographic assessment of [^3H]MK-6884 binding to brain sections from rhesus monkey (Fig. 2A) and human (Fig. 2B) was conducted in the presence of the orthosteric mAChR agonist carbachol (10 μM). Carbachol increases the affinity of [^3H]MK-6884 analogs for the M4R, resulting in better visualization of the brain regions bound (25). The regional binding density of [^3H]MK-6884 was slightly higher in monkey samples than in human samples, with a rank order of density: striatum \gg cortex \approx hippocampus $>$ thalamus \gg cerebellum (Fig. 2C).

Saturation binding studies of [^3H]MK-6884 using crude striatal homogenates from rhesus monkeys and humans were conducted in the presence of 10 μM carbachol. These studies showed that [^3H]MK-6884 binding was saturable and displaceable with dissociation constants (K_d) of 0.9 nM (rhesus monkey) and 1.2 nM (human) (Fig. 2D). The receptor densities (B_{max}) were moderate at 13 nM (monkey) and 7 nM (human), yielding in vitro binding potentials (B_{max}/K_d) of 14.4 (monkey) and 7.8 (human).

PET imaging of [^{11}C]MK-6884 in rhesus monkeys

Concentrations of [^{11}C]MK-6884 in arterial plasma peaked at about 4.5 standardized uptake value (SUV) 2 to 3 min after injection of ≈ 185 MBq of tracer ($n = 3$) and then declined rapidly. [^{11}C]MK-6884 was rapidly metabolized in arterial plasma, with the following percentages of total radioactivity represented by the parent tracer over time after injection in three monkeys: 93.8 \pm 2.1% at 5 min, 60.5 \pm 18.6% at 15 min, 55.1 \pm 6.0% at 45 min, and 39.2 \pm 61.4% at 60 min, as determined by radio-high-performance liquid chromatography (HPLC; fig. S1A). Four radiolabeled metabolites were observed in monkey arterial plasma, with three of these metabolites being more polar, as evidenced by their elution before the parent tracer (fig. S1, B and C). These characteristics suggest that they are unlikely to enter the brain and affect the quantitative analysis of [^{11}C]MK-6884 kinetics. One minor, lipophilic, radiometabolite was observed by HPLC

analysis at a relatively low percentage (<10%) of the total (fig. S1, B and C). The influence of this radiometabolite on the brain signal was considered negligible.

PET studies conducted under baseline conditions showed that [^{11}C]MK-6884 distributed rapidly across the blood-brain barrier, with maximum brain radioactivity (2.0 SUV) achieved within 10 min of tracer injection followed by rapid clearance (Fig. 3, A and B). Regional brain uptake of [^{11}C]MK-6884 was highest in the striatum and is consistent with the results from in vitro autoradiography. Much lower tracer uptake was observed in cortical regions. Pretreating the same monkey with the selective M4 PAM MK-4710 1 hour before injecting [^{11}C]MK-6884 yielded a plasma MK-4710 concentration of 1.2 μM and a corresponding decrease in striatal

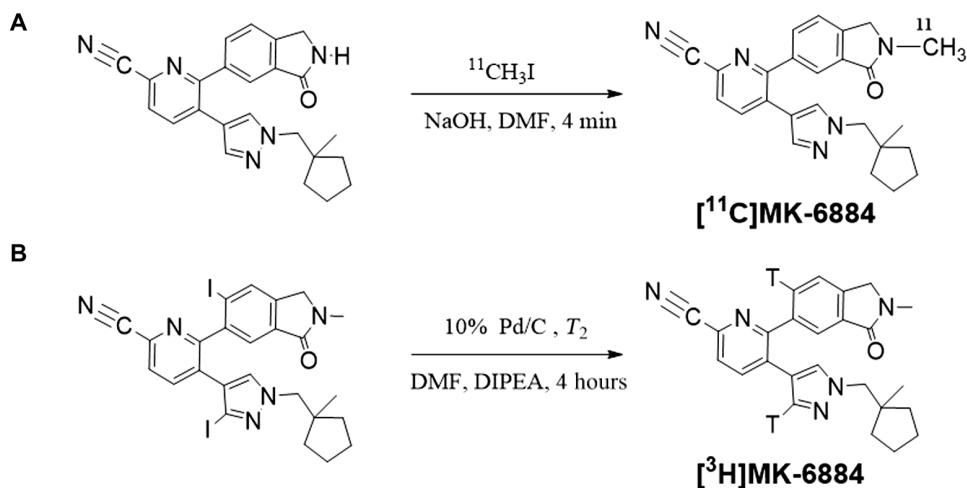


Fig. 1. Radiosynthesis of [^{11}C]MK-6884/[^3H]MK-6884. (A) [^{11}C]MK-6884. (B) [^3H]MK-6884; T: ^3H (tritium). DMF, dimethylformamide; DIPEA, *N,N*-diisopropylethylamine.

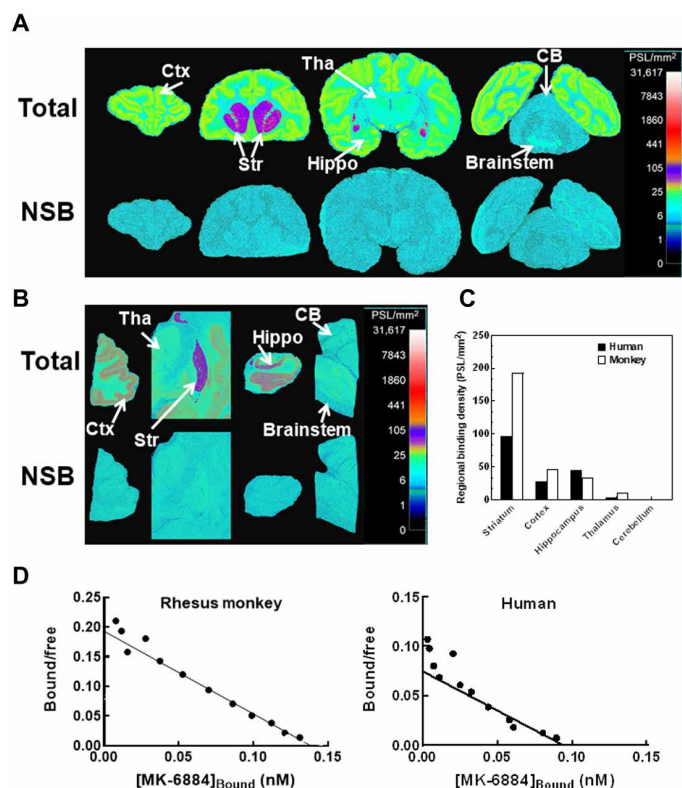


Fig. 2. In vitro characterization of [³H]MK-6884 to brain tissues from rhesus monkey and human. Autoradiographs of [³H]MK-6884 binding to brain sections from (A) rhesus monkey and (B) human. All tissue sections were incubated in the presence of 2 nM [³H]MK-6884 and 10 μ M carbachol. Ctx, cortex; CB, cerebellum; Str, striatum; Tha, thalamus; Hippo, hippocampus; PSL, photostimulated luminescence. The amount of nonspecific binding (NSB) was defined in the presence of 1 μ M MK-6884. (C) Regional binding density in monkey and human tissues. (D) Scatchard plots of [³H]MK-6884 binding to striatal homogenates from rhesus monkey (left) and human (right). B_{max} is expressed in nM relative to wet tissue weight.

radioactivity of about 70% relative to baseline (Fig. 3, A to D). In contrast, the cerebellum time-activity curve (TAC) in the presence of MK-4710 was indistinguishable from baseline (Fig. 3A), indicating the absence of specific [¹¹C]MK-6884 binding in this region. Both the two-tissue compartmental model (2-TCM) with a radiometabolite-corrected arterial input function and the simplified reference tissue model (SRTM) using a reference tissue (cerebellum) free of specific binding yielded similar striatal nondisplaceable binding potential (BP_{ND}) values for [¹¹C]MK-6884 under baseline and blocking conditions (Fig. 3, A, C, and D). These results support the use of the cerebellum as a reference region for the SRTM method of analysis, which was subsequently used in the animal studies.

Repeated baseline scans yielded an average striatal BP_{ND} of 0.83 \pm 0.17 ($n = 10$ scans in five monkeys). The average test-retest variability (T-RT) for the striatal BP_{ND} of [¹¹C]MK-6884 is 7.60 \pm 5.80% (Fig. 3E), which is adequate for quantitative determinations of M4 PAM RO.

Donepezil enhancement of [¹¹C]MK-6884 binding in monkeys

Because the in vitro binding of M4R PAMs is enhanced by orthosteric agonists (e.g., ACh or carbachol) (25, 26), increasing concentrations

of the endogenous orthosteric agonist ACh should also increase the BP_{ND} of [¹¹C]MK-6884 in vivo. This was assessed by administering the acetylcholinesterase inhibitor (AChEI) donepezil (0.1 to 0.3 mg/kg, intramuscularly) before [¹¹C]MK-6884 injection and imaging. The doses of donepezil used were previously found to enhance cognitive function (object retrieval) in scopolamine-impaired rhesus monkeys (27). Donepezil dose-dependently increased the [¹¹C]MK-6884 BP_{ND} in monkey striatum as determined using PET imaging (Fig. 4A), with significant differences between each dose and baseline ($P < 0.05$ for all three doses), leading to maximal enhancement at the dose (0.3 mg/kg). Donepezil (0.3 mg/kg) was subsequently given before administration of the potent, selective, and brain-penetrant M4 PAM compound 1, followed by [¹¹C]MK-6884 injection and scanning. [¹¹C]MK-6884 uptake was dose-dependently reduced by compound 1 in the striatum. For statistical analysis of dose-dependent reduction of [¹¹C]MK-6884 uptakes, SigmaPlot (14.0) was used to perform nonlinear regression of the occupancy versus dose relationship by fitting the Hill equation. The resulting goodness of fit are as follows: with compound 1 alone, $R_{sq} = 0.6600$ (Adj $R_{sq} = 0.6034$); with compound 1 in the presence of donepezil, $R_{sq} = 0.6160$ (Adj $R_{sq} = 0.5777$). The potency (Occ_{50}) of compound 1 in occupying the M4Rs increased about 2.5-fold in the presence of donepezil ($Occ_{50} = 170 \pm 34$ nM) relative to that of compound 1 alone ($Occ_{50} = 430 \pm 91$ nM; Fig. 4B).

Clinical PET imaging studies with [¹¹C]MK-6884

Phase 1 studies validating [¹¹C]MK-6884 as an M4R-specific PET tracer were conducted in healthy human participants to determine radiation dosimetry ($n = 3$), regional brain distribution, baseline T-RT variability ($n = 6$), binding modulation by donepezil ($n = 8$), and target engagement ($n = 13$; table S1). Whole-body images showed radioactivity distributed throughout the heart, brain, and liver shortly after administration of 133 to 360 MBq (≤ 4.9 μ g) of [¹¹C]MK-6884, which was rapidly cleared by hepatic and renal routes (fig. S1 and table S2). Administration of 300 MBq of [¹¹C]MK-6884 yielded a human effective dose of ≈ 2.2 mSv.

The kinetics of tracer distribution through multiple brain regions were investigated in healthy elderly participants. [¹¹C]MK-6884 showed rapid, heterogeneous distribution into the brain (Fig. 5, A and B). TACs were similar for the striatum and cortical regions and peaked at two to three SUVs 3 min after administration before rapidly declining. Hippocampal TAC displayed a lower peak and slower clearance. Regional BP_{ND} yielded a rank order of striatum \approx cortex > hippocampus > cerebellum (Fig. 5, A to C). This differs from rhesus monkeys, as a much lower BP_{ND} was observed in the cortex and hippocampal regions (average $BP_{ND} \leq 0.10$; Fig. 3B). The metabolism of [¹¹C]MK-6884 is faster in humans than in monkeys, with 74 \pm 15% ($n = 6$) of plasma radioactivity at 5 min after dose represented by [¹¹C]MK-6884, decreasing to 27 \pm 7.6% ($n = 6$, mean \pm SD) at 90 min after dose (fig. S3A). The major metabolic pathway produced primarily polar metabolites. More lipophilic radiometabolites were not observed in human plasma samples, although it is possible that they were not revealed in our assays because of its detection limits (fig. S3B). The conventional two-tissue compartment model did not yield stable total volume of distribution (V_T) estimates for the brain regions analyzed, which may be attributable to a brain-penetrant radiometabolite. Instead, the data are better described by 1-TCM with arterial input function (fig. S3), the reference tissue model (SRTM using cerebellum), and the transient equilibrium tissue ratio

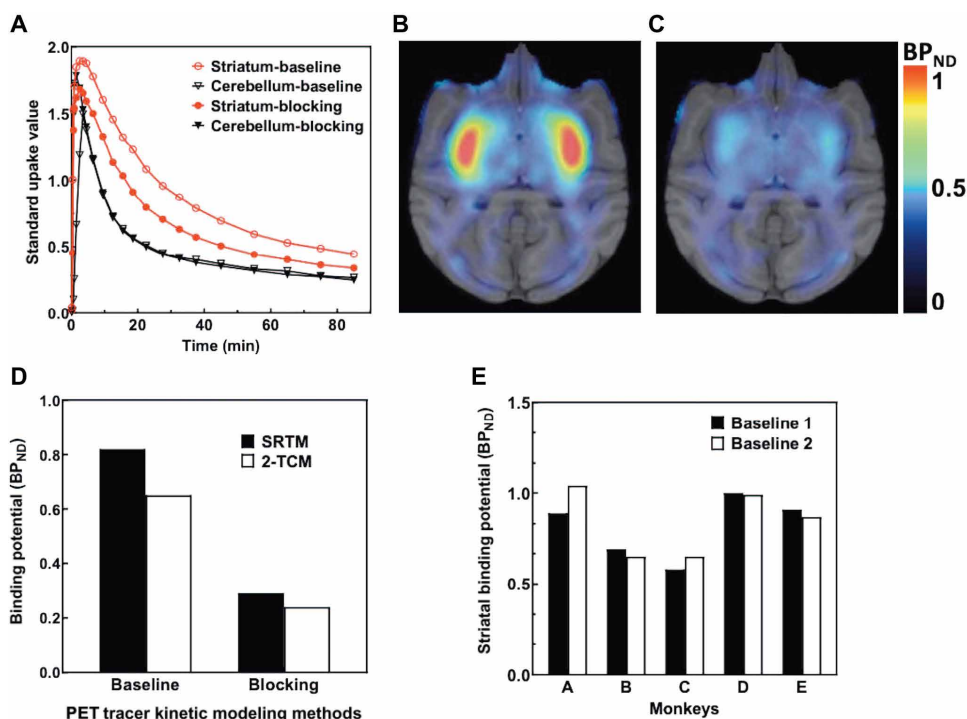


Fig. 3. Characterization of [^{11}C]MK-6884 binding to the brain under baseline and blocking conditions using PET imaging of rhesus monkeys. (A) [^{11}C]MK-6884 TACs in rhesus monkey striatum (circles) and cerebellum (triangles) at baseline (open symbols) and after the administration of MK-4710 (closed symbols). (B) Co-registered, transverse plane baseline PET/MRI image of [^{11}C]MK-6884 uptake in rhesus monkey brain, with the highest tracer binding localized in the striatum. (C) Image taken after administration of MK-4710 1 hour before [^{11}C]MK-6884. The color scale represents the magnitude of BP_{ND} . (D) Striatal BP_{ND} determined under baseline and blocking conditions using SRTM (closed columns) and 2-TCM (open columns). (E) Comparison of striatal BP_{ND} values for determination of T-RT variability in five monkeys.

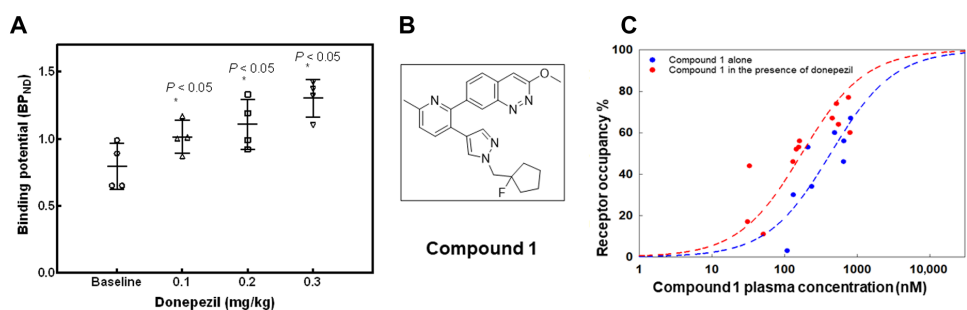


Fig. 4. The effect of donepezil on the BP_{ND} of [^{11}C]MK-6884 and the RO of compound 1 in the striatum of rhesus monkeys determined in vivo. (A) Relationship between the mean striatal BP_{ND} of [^{11}C]MK-6884 and the plasma concentration of donepezil. * $P < 0.05$, analysis of variance (ANOVA) followed by Tukey's post hoc analysis. (B) Compound 1, 7-[3-[1-[(1-fluorocyclopentyl)methyl]pyrazol-4-yl]-6-methyl-2-pyridyl]-3-methoxycinnoline. (C) Relationship between the plasma concentration of compound 1 and M4 RO determined in rhesus monkey striatum ($n = 5$) using [^{11}C]MK-6884 PET imaging performed in the presence (red curve) and absence (blue curve) of donepezil (0.3 mg/kg, intramuscularly).

(TE-TR) models. All three models provided comparable BP_{ND} values for striatum, frontal cortex, temporal cortex, and hippocampus (Fig. 5C), with the TE-TR method yielding a striatal BP_{ND} of 0.96 ± 0.13 ($n = 6 \pm \text{SD}$) and intra-individual T-RT variability of about 11% (Fig. 5D). Therefore, the TE-TR method was subsequently used for data processing.

[^{11}C]MK-6884 PET occupancy studies were conducted in 13 human subjects to quantify the extent of target engagement achieved by the highest tolerated single dose of the M4 PAM MK-4710 (fig. S4). [^{11}C]MK-6884 showed plasma concentration and time-dependent reductions in brain uptake and striatal BP_{ND} after MK-4710 dosing relative to baseline (Fig. 6, A and B). The relationship between average MK-4710 plasma concentrations versus M4R occupancies from PET studies at 10 hours after oral dosing of MK-4710 was best fitted by a sigmoidal, two-parameter Hill equation ($E_{\text{max}} = 100\%$) with an Occ_{50} of 340 ± 170 nM (mean \pm SE; Fig. 6C). The RO achieved with the maximally tolerated single dose (10 mg, orally) of MK-4710 increased from $34 \pm 2.1\%$ at 2 hours after dose to a maximum of $43 \pm 8.0\%$ at ≈ 6 hours, declining to $27 \pm 7.8\%$ by 52 hours after dose.

The effect of donepezil on [^{11}C]MK-6884 binding was studied in healthy elderly participants administered an accelerated titration dosing regimen of donepezil over 21 days (fig. S5). No difference in the magnitude of striatal BP_{ND} was observed on days 4 and 9 of donepezil administration. However, the striatal BP_{ND} of [^{11}C]MK-6884 showed a 23% ($n = 7$) increase above baseline on day 22 (1.2 ± 0.17 , $P < 0.05$) (Fig. 6, D and E). In contrast, the BP_{ND} of [^{11}C]MK-6884 in the frontal and temporal cortices in the presence of donepezil did not show an increase at any time point (frontal cortex, baseline: 0.89 ± 0.17 ; day 22: 0.98 ± 0.17) (table S3). The changes in striatal BP_{ND} positively correlated with donepezil plasma concentrations, although an inverse relationship was observed between the change in BP_{ND} and the degree of erythrocyte acetylcholinesterase activity (fig. S7).

Regional BP_{ND} of [^{11}C]MK-6884 in patients with AD

The distribution of [^{11}C]MK-6884 in the striatum of patients with AD stably treated with either donepezil or rivastigmine was bilaterally symmetric and homogeneous, with an average striatal BP_{ND} of $0.98 \pm$

0.20 ($n = 10$; Fig. 7, A and B). This value is comparable to the striatal BP_{ND} observed in healthy elderly participants under baseline conditions (0.97 ± 0.18 ; Fig. 7B). However, the striatal BP_{ND} in healthy elderly subjects treated with the donepezil titration dosing regimen (1.20 ± 0.17) was about 24% higher than in patients with AD ($P < 0.01$). In contrast, [^{11}C]MK-6884 uptake by the cortex was

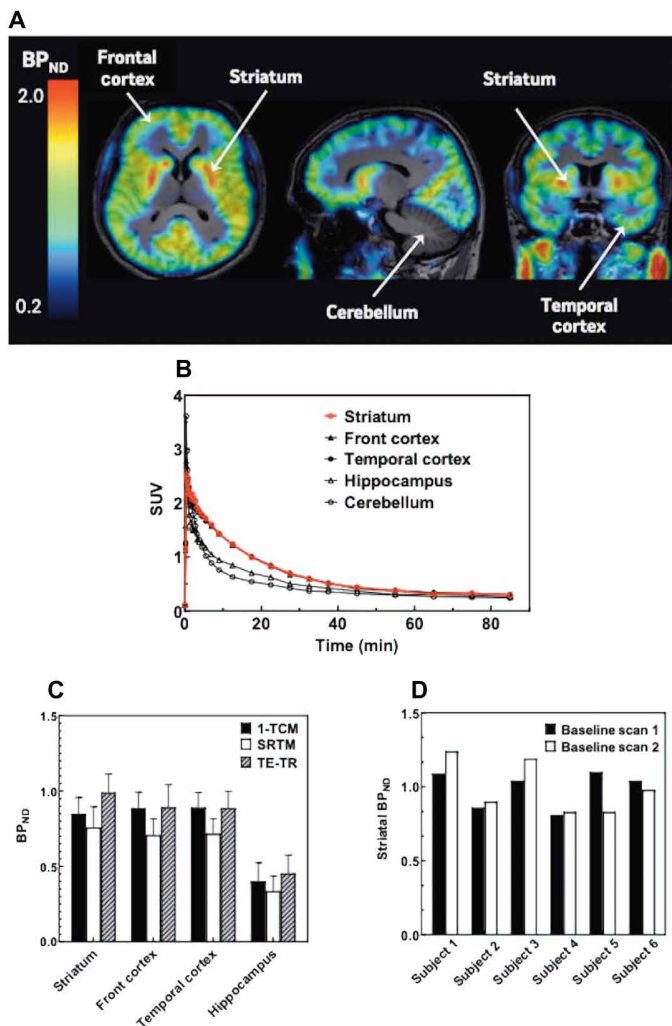


Fig. 5. PET imaging of [¹¹C]MK-6884 uptake in healthy human brain. (A) Representative, derived PET parametric (BP_{ND}) brain images of [¹¹C]MK-6884 in a healthy adult brain under baseline conditions. Images are superimposed upon MR images from the same subject and presented in coronal, sagittal, and transverse planes. (B) Representative regional TACs from a healthy adult administered [¹¹C]MK-6884 at baseline: striatum (red circles), frontal cortex (filled triangles), temporal cortex (filled circles), hippocampus (open triangles), and cerebellum (open circles). (C) Regional BP_{ND} determined under baseline conditions using 1-TCM, SRTM, and TE-TR. (D) Comparison of striatal BP_{ND} values for determination of T-RT variability in six human subjects using TE-TR method.

regionally heterogeneous in patients with AD, and the BP_{ND} in both frontal and temporal cortices showed no significant difference between healthy elderly participants and patients with AD (frontal cortex: 0.92 ± 0.15 versus 0.74 ± 0.20 , healthy versus AD, respectively; $P = 0.07$; Fig. 7B). There was a significant difference of temporal cortex BP_{ND} between healthy elderly participants and patients with AD (0.83 ± 0.15 versus 0.46 ± 0.18 , healthy versus AD, respectively; $P < 0.01$; Fig. 7B.) This heterogeneity in cortical uptake was observed in all patients with AD scanned (Fig. 7B). There was no significant positive correlation between the Mini-Mental Status Exam (MMSE) score of patients with AD at the time of the scan and the striatal (Pearson $r = 0.31$, $P = 0.19$), temporal cortical (Pearson $r = 0.26$, $P = 0.23$), and frontal cortex (Pearson $r = 0.53$, $P = 0.058$; table S4).

DISCUSSION

[¹¹C]MK-6884 was developed as a PET tracer for determining the degree of target engagement by allosteric modulators of the M4R under development for the treatment of NPS associated with AD. An off-target screen (Eurofins Panlabs) indicated that MK-6884 preferentially binds with high affinity to the M4R over 115 other targets (25). The pharmacology of MK-6884 is consistent with a PAM, as indicated by radioligand binding assays conducted in the presence of the orthosteric agonist carbachol, which increased the affinity of [³H]MK-6884 binding. Addition of carbachol to the binding assays better revealed that the regional localization of binding is consistent with known M4R mRNA and protein expression (10), with the highest density in the striatum and intermediate amount of expression in the cortex, hippocampus, and thalamus.

Given the high affinity and target selectivity of MK-6884, pre-clinical imaging studies were conducted in vivo, which further validate the suitability of [¹¹C]MK-6884 as a PET tracer for clinical applications. Co-administration of either MK-4710 or compound 1 dose-dependently reduced [¹¹C]MK-6884 binding to monkey striatum relative to the cerebellum. Furthermore, these studies demonstrated the utility of [¹¹C]MK-6884 in determining target engagement by the M4 PAM MK-4710 in clinical applications. Additional evidence that the pharmacology of [¹¹C]MK-6884 as a PAM was maintained in vivo was provided by administering the AChEI donepezil to increase brain ACh quantities (28, 29). At doses of donepezil that enhance cognitive performance in scopolamine-treated monkeys, the striatal BP_{ND} of [¹¹C]MK-6884 increased about 60% above baseline, indicating that regional uptake of the PET tracer is sensitive to changes in cholinergic tone. Considering that the B_{max}/K_d in vitro is proportional to the specific in vivo signal and assuming that acute donepezil administration does not alter M4R density (B_{max} is unchanged), the increase in striatal BP_{ND} reflects an increase in the affinity of [¹¹C]MK-6884 for the M4R.

Overall, the in vitro and in vivo pharmacology of MK-6884 in monkeys was predictive of its performance as a PET tracer in humans in terms of whole-body distribution, signal-to-noise ratio, clearance, brain regional localization, allosteric modulation, and competitive binding. One notable difference is that baseline cortical binding in humans is greater than observed in monkeys. Whereas donepezil treatment increased the striatal BP_{ND} of [¹¹C]MK-6884 above baseline, cortical BP_{ND} was relatively unchanged. This may be due to the greater dynamic range associated with the striatal SUV, which might better reveal allosteric modulation of [¹¹C]MK-6884 uptake in vivo than in the cortex.

Another factor affecting striatal [¹¹C]MK-6884 binding and the therapeutic efficacy of M4 PAMs is the loss of cholinergic pathways in AD. The striatal BP_{ND} of [¹¹C]MK-6884 in patients with AD receiving an AChEI was similar to that of healthy, age-matched subjects at baseline. This may be due to the relative integrity of cholinergic interneurons and signaling pathways (30–33) in the striatum rather than in the cortex of patients with AD. However, the striatal BP_{ND} in patients was lower than observed in healthy elderly subjects treated with donepezil. This may reflect a secondary loss of corticostriate projections with resultant decreases in presynaptically localized M4R (10, 12) over the course of the disease, a process that may be monitored in longitudinal studies during disease progression in patients with AD. Alternatively, striatal ACh concentrations may be lower in patients, leading to decreased ligand binding affinity. Regardless, if the population of striatal M4R in patients with AD is unchanged

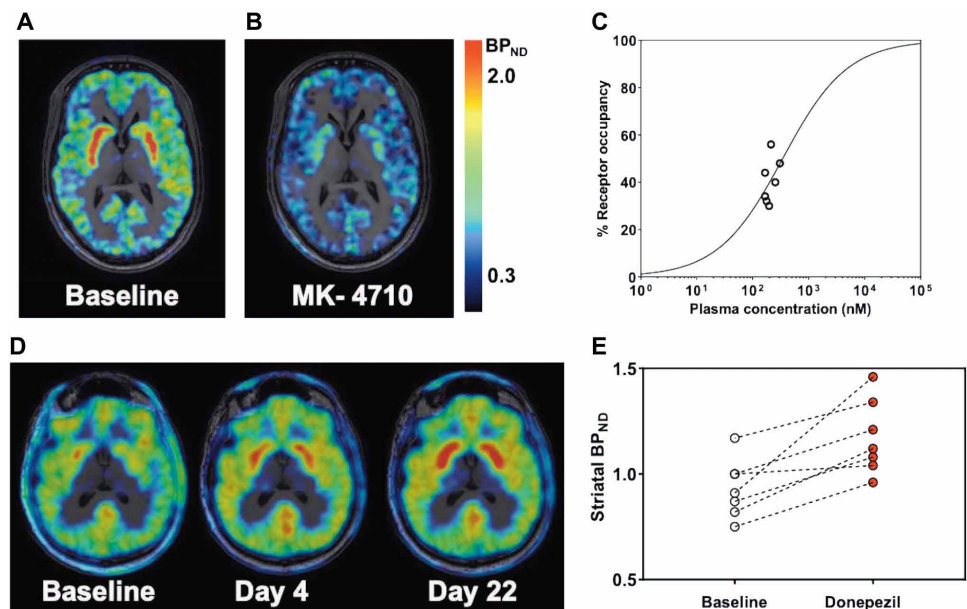


Fig. 6. Target engagement and modulation of [¹¹C]MK-6884 BP_{ND} in healthy volunteers. (A) Representative scan of a healthy adult volunteer taken under baseline conditions. (B) PET image from the same subject ≈10 hours after oral administration of 10 mg of MK-4710. (C) Relationship between plasma concentrations of MK-4710 and the percentage RO by [¹¹C]MK-6884 ≈10 hours after administration of MK-4710. Each point represents the RO determined from an individual scan. (D) Representative PET scans taken from the same healthy elderly participant illustrating regional changes in [¹¹C]MK-6884 BP_{ND} with donepezil intervention at baseline, on day 4 (5 mg), and on day 22 (last dose of 10 mg on day 21) of treatment with an accelerated donepezil titration dosing regimen. (E) Comparison of striatal BP_{ND} of [¹¹C]MK-6884 in healthy elderly volunteers between baseline and after 21 days of donepezil treatment.

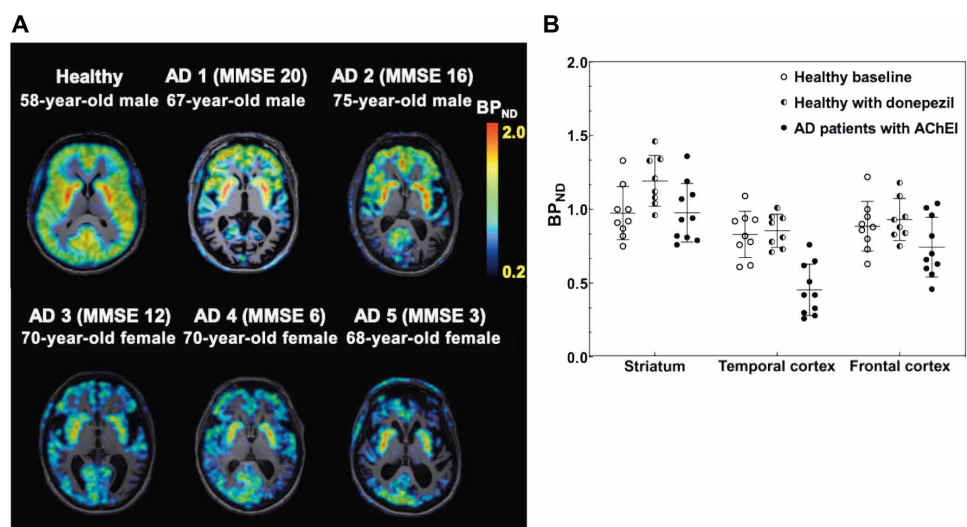


Fig. 7. Regional differences in the BP_{ND} of [¹¹C]MK-6884 in AD patients receiving AChEI therapy compared to age-matched, healthy elderly volunteers receiving donepezil treatment. (A) Representative scans of a healthy adult volunteer taken under baseline conditions and patients with AD with MMSE scores ranging from 3 to 20 receiving AChEI treatment. (B) Comparison of BP_{ND} values for [¹¹C]MK-6884 binding to the striatum, temporal, and frontal cortices of healthy adults (18 to 55 years of age, open circles) under baseline conditions after 21 days of donepezil treatment (half-filled circles) and in patients with AD (filled circles) receiving either donepezil or rivastigmine therapy. ANOVA and Tukey's multiple comparison test was performed.

relative to healthy participants (10), or if their function is normalized by administration of an AChEI, the ability of these neurons to regulate striatal dopaminergic neurotransmission may continue to be a substrate for modulation by M4 PAMs in the treatment of NPS (9, 34–37).

In contrast with the striatum, the density of cortical M4R appears to be strongly affected by the loss of efferent pathways from the nucleus basalis (10, 18, 38), a pathognomonic change associated with AD. Previous investigations of cortical necropsy specimens from AD donors variously report increases, decreases, or no changes in muscarinic receptor densities, depending on the cortical region, method of measurement (radioligand binding or immunochemistry), and severity of disease (19–21). Whereas the striatal BP_{ND} of patients with AD treated with an AChEI was similar to that of healthy adults, cortical BP_{ND} values were substantially decreased by subregion, with the area and extent of change varying individually. This may reflect the loss of presynaptic M4R residing on cholinergic or glutamatergic terminals (10), with an average decrease of ≈20% in frontal cortex BP_{ND} of individuals with AD compared to healthy adults. This is consistent with limits to the ability of AChEI treatment to maintain cortical M4R functionality in the face of disease progression (39).

The BP_{ND} in the frontal cortex of subjects with AD is only weakly correlated with the MMSE score, with no relationship shown between other cortical regions and MMSE score. Although the weak relationship between cortical binding and MMSE score may reflect the small number of patients investigated and absence of partial volume correction, these results trend in the direction of previous observations of decreases in the regional binding density of PET ligands for the synaptic vesicle 2A protein in patients with AD (40, 41), where correlations between MMSE score and ligand distribution were found in the hippocampus, prefrontal, and temporal cortices (41). Furthermore, given the involvement of muscarinic cholinergic receptors in higher-order visual perception (42–44), the substantial decreases in BP_{ND} in the parietal and occipital cortices may contribute to deficits in visuospatial processing commonly observed in patients

with AD (45) and may correlate better with scores from tests of visuospatial processing.

There are several limitations to our study. Our primary cohort of patients is relatively small, with only 10 male and female individuals with moderate-to-severe AD (MMSE \leq 20, 6 patients with MMSE \geq 14). This is, in part, due to the challenge of recruiting elderly and severe patients to undergo diagnostic medical imaging, despite the lack of therapeutic interventions. Given the small sample and the heterogeneity of the brain regions, with the occipital cortex being the neocortical area most resistant to AD pathology, the MMSE correlation with cortical regional BP_{ND} as discussed above was underpowered to validate a predictive biomarker. In addition, in this study, we were unable to identify patients without prior AChEI treatments, as all 10 of them were stably maintained on either donepezil or rivastigmine for at least 4 weeks. These issues suggest that further analysis of the relationship between tests of cognitive function and the BP_{ND} of [¹¹C]MK-6884 in cortical and hippocampal regions is warranted in a more extensive longitudinal study in a larger cohort.

In conclusion, [¹¹C]MK-6884 is a selective M4R PET tracer with pharmacological properties consistent with a PAM. It is displaceable by other M4 PAMs, and its binding is modulated by the orthosteric ligands ACh and carbachol in both primate and human. These attributes make it a suitable tool for assessing direct target engagement by competitive allosteric modulators interacting with the same binding site and for providing proof of biology for orthosteric ligands modulating M4R function. The availability of [¹¹C]MK-6884 should aid in the development of other M4R selective ligands for therapeutic indications. Moreover, the ability of [¹¹C]MK-6884 to reveal regional changes in M4R density and/or ACh tone (and potentially, functionality) in patients with AD suggests that it may provide insights into the neurotransmitter-specific pathology of the disease.

MATERIALS AND METHODS

Study design

The goal of this study was to assess [¹¹C]MK-6884 as a PET tracer for measuring target engagement in human brain and providing insights into neuropathology in patients with AD. We characterized [³H]MK-6884/[¹¹C]MK-6884 binding in vitro (brain tissues) or in vivo (in monkeys) before clinical translation. Then, we validated the utility of [¹¹C]MK-6884 in healthy subjects and individuals with AD (ClinicalTrials.gov: NCT02621606). Sample sizes for both nonclinical and clinical investigations were determined empirically. All clinical studies were conducted in adherence with the standards of Good Clinical Practice. Stop dosing criteria in the clinical studies were based solely on safety parameters [electrocardiograms (ECGs), vital sign measures, and adverse event reporting]. This established the maximum tolerated dose of MK-4710 at 10 mg, with the discontinuation of one participant in study MK-6884-002 because of syncope associated with donepezil treatment. No data were excluded from analysis or considered an outlier. Clinical endpoints were selected prospectively. The number of replicates in each experiment is indicated in the appropriate sections. Research objectives, subjects, experimental design, randomization, and blinding of each clinical study are described in the “Clinical PET imaging studies with [¹¹C]MK-6884” section below. All clinical study participants or their legal guardians were informed of the nature of the study and the potential risks of

the investigation before providing written consent. All clinical investigations were approved by regionally appropriate Institutional Review Boards. None of the clinical trials described in this article were blinded, nor were the participants randomized to treatments.

Radiochemistry of [¹¹C]MK-6884 and [³H]MK-6884

Figure 1 (A and B) shows the synthetic scheme for preparation of [¹¹C]MK-6884/[³H]MK-6884. Details of the radiosynthesis are provided in the Supplementary Materials.

In vitro characterization of [³H]MK-6884 binding to brain tissues

The distribution and specificity of [³H]MK-6884 binding to brain sections from mouse (wild-type and M4R knockout), rhesus monkey, and human brain were determined using previously reported autoradiographic techniques (46). Details of methods used to conduct the autoradiography and saturation binding studies using striatal homogenates prepared from rhesus monkeys and human controls can be found in the Supplementary Materials. A nonlinear regression fit of a rectangular hyperbola to the resulting data was used to determine K_d and B_{max} (GraphPad Prism version 8.2.1). The [³H]MK-6884 B_{max} values in nmol/mg tissue wet weight were converted to B_{max} (nM) values by multiplying the tissue dilution factor by wet tissue weight in the assay.

PET imaging studies in rhesus monkeys

All monkey PET imaging studies were conducted according to guidelines from the American Physiological Society and the *Guide for the Care and Use of Laboratory Animals* (National Institutes of Health publication no. 85-23, revised 2010) and were approved by the Research Laboratories of Merck & Co. Inc. The animal preparation, baseline PET scan acquisition, and image analysis used were similar to methods described previously (25). Briefly, five rhesus monkeys (age range 5 to 9, \approx 7 to 14 kg, two male and three females) were initially sedated with ketamine (10 mg/kg, intramuscularly), induced with propofol (5 mg/kg, intravenously), intubated, and then respired with a medical-grade air and oxygen mixture at \approx 10 ml per breath per kilogram and 23 respirations per minute. Anesthesia was maintained with propofol (0.4 to 0.55 mg/kg per minute) for the duration of the study. Body temperature was maintained with circulating water heating pads, and temperature, oxygen saturation, blood pressure, and end-tidal CO₂ were monitored for the duration of the study. Dynamic PET scans were acquired in a PET/CT or HR+ scanner (Siemens) over 90 min after a 2-min bolus intravenous injection of [¹¹C]MK-6884 (\approx 185 MBq, $<$ 2 μ g). Whole-blood samples were collected via arterial catheter into heparin tubes for determination of radioactivity in whole-blood and plasma. Samples are centrifuged, and 20 μ l of whole blood and plasma was counted in a gamma counter at 10, 20, 30, 45, 60, 90, and 120 s after [¹¹C]MK-6884 injection. Samples of blood (0.5 ml) were taken at 3, 5, 15, 30, 60, and 90 min for determination of in vivo metabolism of the tracer and total radioactivity in plasma and whole blood. The plasma concentration of [¹¹C]MK-6884 was determined from measures of total radioactivity in arterial plasma with correction for the fraction of intact tracer as determined by radio-HPLC analysis. Reconstructed images were aligned with magnetic resonance imaging (MRI)-based templates for each monkey, and TACs were drawn on the PET images to quantify the regional tracer uptake SUV and BP_{ND} using TCMs. Repeat baseline PET scans were conducted in these same monkeys.

Comparison of BP_{ND} determinations using below equation from five different monkeys provided the average T-RT variability

$$\text{T-RT variability} = 2 \times \frac{|BP_{ND}^{\text{Baseline 1}} - BP_{ND}^{\text{Baseline 2}}|}{|BP_{ND}^{\text{Baseline 1}} + BP_{ND}^{\text{Baseline 2}}|}$$

For M4R blockade scans, the potent and selective brain-penetrant M4R PAM MK-4710 was intravenously administered as a bolus (1.68 mg/kg) followed by an infusion (0.96 mg/kg per hour) starting 1 hour before [^{11}C]MK-6884 injection. Because the cerebellum is devoid of M4R, SRTM using cerebellum as the reference region was applied to determine striatal BP_{ND} .

Enhancement of [^{11}C]MK-6884 binding in monkeys by donepezil

To assess the effect of endogenous ACh on the BP_{ND} of [^{11}C]MK-6884 in vivo, a crossover PET study was performed in rhesus monkeys ($n = 4$) by pre dosing with donepezil to increase the ACh concentrations before administration of [^{11}C]MK-6884. The animal preparation, PET scan acquisition, and image analysis were similar to the methods described above. Donepezil was intramuscularly administered in doses of 0.1, 0.2, or 0.3 mg/kg 1 hour before [^{11}C]MK-6884 injection. Dynamic PET scans were acquired in a PET/CT or HR+ scanner (Siemens) over 90 min after [^{11}C]MK-6884 (≈ 185 MBq, < 2 μg) injection. Venous plasma samples were collected serially during the scan period to measure contemporaneous plasma concentrations of donepezil matched to the striatal BP_{ND} determined from each scan using SRTM. The striatal BP_{ND} associated with donepezil doses ($n = 3$) versus baseline values was used to identify the dose of donepezil causing maximal enhancement. This dose of donepezil was subsequently used to determine whether the plasma concentration/RO relationship in monkeys was shifted by the ACh concentration in brain. Briefly, donepezil (0.3 mg/kg) or saline was intramuscularly administered to the right thigh muscle. At the same time, doses of compound 1 were intravenously administered as bolus plus infusion (0.16/0.07 to 1.00/0.42 mg/kg per hour) in vehicle containing 1% 1 N HCl and 30% Captisol 1 hour before [^{11}C]MK-6884 injection. PET scans were collected for 90 min, and striatal BP_{ND} was determined using previously described techniques. From each treatment scan, compound 1 post-administration versus baseline (no-drug) striatal BP_{ND} values were used to obtain RO % using the equation below

$$\text{RO (\%)} = \frac{(\text{Baseline } BP_{ND} - \text{PostDrug } BP_{ND})}{\text{Baseline } BP_{ND}} * 100$$

The % RO and the average plasma concentration of compound 1 in the absence or presence of donepezil were fitted with a sigmoidal E_{max} model to determine Occ_{50} and Hill slope h .

Clinical PET imaging studies with [^{11}C]MK-6884 MK-6884-001 (ClinicalTrials.gov registration number: NCT02621606)

This was an open-label study conducted in three parts. Part I assessed the safety, tolerability, and tracer characteristics of [^{11}C]MK-6884 in three healthy adult males and females, 18 to 55 years of age. A series of whole-body PET scans, clinical examinations, and laboratory safety evaluations were conducted after administration of a single previously defined intravenous dose of [^{11}C]MK-6884 of 370 MBq (10 mCi, ≤ 4.9 μg) of [^{11}C]MK-6884.

Part II was performed in seven healthy elderly male and female subjects 55 to 85 years of age and evaluated the safety and tolerability of two intravenous doses of [^{11}C]MK-6884, determined its distribution kinetics throughout the brain (V_T), established baseline M4R availability, and determined the intrasubject baseline T-RT variability of brain M4R BP_{ND} by performing a dynamic PET scan of about 90-min duration after administration of [^{11}C]MK-6884 on two separate occasions. The regional brain TACs for all subjects were fitted by compartmental modeling with metabolite-corrected arterial input functions to obtain V_T (tissue/plasma concentration ratio at equilibrium). Baseline T-RT variability was determined using the following equation

$$\text{TRV} = 2 \times \frac{V_T^{\text{scan1}} - V_T^{\text{scan2}}}{V_T^{\text{scan1}} + V_T^{\text{scan2}}}$$

Arterial blood was sampled for measuring concentrations of parent radiotracer and metabolites for quantification of tracer kinetic modeling methods. Target BP_{ND} was determined using the cerebellum as the reference region with both the SRTM and TE-TR methods.

Part III evaluated the brain distribution of [^{11}C]MK-6884 BP_{ND} in 10 male and female patients (55 to 85 years of age) with moderate-to-severe AD (MMSE ≤ 20), age-matched to the healthy elderly subjects in part II. All patients with AD were stably maintained on either donepezil or rivastigmine for at least 4 weeks before screening. An MRI scan of the brain was obtained for delineation of regions of interest (ROIs) and to validate the diagnosis of moderate-to-severe AD. Each patient was administered a single intravenous dose of ≈ 370 MBq of [^{11}C]MK-6884, and a single brain scan was performed over ≈ 90 min to determine the BP_{ND} of [^{11}C]MK-6884. Blood samples for AChE plasma concentration and red blood cell-AChE activity were measured before [^{11}C]MK-6884 dosing.

MK-6884-002

This was an open-label, two-cohort investigation of the effect of donepezil on the regional BP_{ND} of [^{11}C]MK-6884 in the brain. Males and females 55 to 85 years of age were randomly allocated to one of two cohorts of four subjects each for donepezil intervention (fig. S4). On day 0, all participants underwent an MRI to delineate ROI and then were administered a tracer dose of [^{11}C]MK-6884 followed by a PET scan to establish baseline BP_{ND} . Subsequently, both cohorts were started on the same donepezil regimen (5 mg once daily $\times 7$ days followed by 10 mg once daily $\times 14$ days). Because each participant was limited to a total of three PET scans, scanning was staggered by cohort. Cohort 1 was scanned on day 4, at the end of 4 days of 5-mg donepezil treatment, whereas cohort 2 was scanned on day 9, after 2 days of 10-mg donepezil treatment. Both cohorts were scanned again on day 22 after completing the 21 days of donepezil treatment. A pharmacokinetic (PK)/pharmacodynamic (PD) model predicting the relationship between plasma donepezil concentration and brain AChE activity was constructed with published data (47, 48) and used to determine the optimal dates for scheduling PET scans. Because of circadian variation in ACh amounts, all scans were conducted at about the same time of day (between 12:00 and 17:00 hours).

Plasma donepezil concentrations were assessed at baseline and before administration of [^{11}C]MK-6884 at each subsequent PET scan. The PD effects of donepezil were monitored by measuring RBC-AChE activity.

MK-4710-003

This was an open-label PET study characterizing the temporal relationship between the plasma concentration of the M4 PAM MK-4710 administered orally and the degree of striatal RO. The study enrolled 13 healthy adult males between 18 and 50 years of age, who were treated according to the schedule in fig. S5. Each subject underwent a pre-dose MRI scan of the brain, a baseline PET scan, and up to three additional post-dose PET scans in the presence of MK-4710 for a total of up to four PET scans per subject [total exposure to MK-6884 per subject: $\leq 19.6 \mu\text{g}$ ($1/100$ th the no observed adverse effect level) 7.49 mSv (annual exposure limit = 10 mSv)]. Subjects could be dosed twice with MK-4710 on two separate occasions with a washout of at least 7 days between doses.

Subjects were administered [^{11}C]MK-6884 ($\approx 260 \text{ MBq}$, $\approx 7.0 \text{ mCi}$, $\leq 4.9 \mu\text{g}$ per dose) by intravenous bolus and underwent baseline or post-dose scans lasting $\approx 90 \text{ min}$. For determination of the kinetics of MK-4710 dissociation from the M4R, two PET scans were acquired at 2 and 22 hours after dosing with 8 mg of MK-4710. Two subjects received arterial catheters for blood sampling during baseline and post-dose PET scans to validate the models used for PET tracer quantification. Vital sign, 12-lead ECG (single records), and blood draws for laboratory safety tests were taken just before and after each scan, regardless of period or scan number, and at the study exit exam. For each post-dose scan, RO was determined by calculating the changes in the striatal BP_{ND} between baseline and receptor-blocked conditions using the same above equation as used in the rhesus monkey RO study. The average plasma concentration of MK-4710 during the PET scan was correlated with the RO measured from PET images, with a sigmoidal E_{max} model fitted to the data to determine Occ_{50} and Hill slope h .

Statistical analyses

MK-6884-001: One-tailed Pearson's correlation coefficients for the relationship between MMSE score and regional [^{11}C]MK-6884 BPND were determined using GraphPad Prism (version 8.2.1).

MK-6884-002: A linear mixed effects model with day and sex/gender as the fixed effects and subject as the random effect was used to evaluate the primary hypothesis that the BPND of [^{11}C]MK-6884 in the brain region with the highest M4 receptor density is increased by a donepezil intervention regimen titrated to achieve therapeutic effects at steady state. Least-squares estimates and 90% confidence intervals (CIs) for the mean change from baseline were computed at each post-dose time point using the mean squared error from the model and referencing a t -distribution. If the 90% CI for the mean change from baseline on day 22 was greater than 0, then the primary hypothesis that the BPND of [^{11}C]MK-6884 is increased when a single dose of tracer is co-administered with the donepezil intervention regimen at steady state (day 22) is supported. The secondary hypothesis that the BPND of [^{11}C]MK-6884 is increased when a single dose of tracer is co-administered at intermediate time points during the donepezil intervention regimen is supported if the 90% CIs for the mean change from baseline on days 4 and 9 both lie above 0. Linear regression analyses were used to determine the population PK/PD relationship between the striatal BPND of [^{11}C]MK-6884 and plasma donepezil concentrations, as well as with erythrocyte AChE activity.

MK-4710-003: For statistical analysis of dose-dependent reduction of [^{11}C]MK-6884 uptakes in healthy subjects, SigmaPlot (version 14.0) was used to perform nonlinear regression of the occupancy versus dose relationship by fitting the Hill equation.

SUPPLEMENTARY MATERIALS

www.science.org/doi/10.1126/scitranslmed.abg3684

Materials and Methods

Figs. S1 to S7

Tables S1 to S4

[View/request a protocol for this paper from Bio-protocol.](#)

REFERENCES AND NOTES

1. K. L. Lanctôt, J. Amatniek, S. Ancoli-Israel, S. E. Arnold, C. Ballard, J. Cohen-Mansfield, Z. Ismail, C. Lyketsos, D. S. Miller, E. Musiek, R. S. Osorio, P. B. Rosenberg, A. Satlin, D. Steffens, P. Tariot, L. J. Bain, M. C. Carrillo, J. A. Hendrix, H. Jurgens, B. Boot, Neuropsychiatric signs and symptoms of Alzheimer's disease: New treatment paradigms. *Alzheimers Dement.* **3**, 440–449 (2017).
2. M. Steinberg, H. Shao, P. Zandi, C. G. Lyketsos, K. A. Welsh-Bohmer, M. C. Norton, J. C. S. Breitner, D. C. Steffens, J. T. Tschanz; Cache County Investigators, Point and 5-year period prevalence of neuropsychiatric symptoms in dementia: The Cache County Study. *Int. J. Geriatr. Psychiatry* **23**, 170–177 (2008).
3. N. Herrmann, K. L. Lanctôt, Pharmacologic management of neuropsychiatric symptoms of Alzheimer disease. *Can. J. Psychiatry* **52**, 630–646 (2007).
4. N. C. Bodick, W. W. Offen, A. I. Levey, N. R. Cutler, S. G. Gauthier, A. Satlin, H. E. Shannon, G. D. Tollefson, K. Rasmussen, F. P. Bymaster, D. J. Hurley, W. Z. Potter, S. M. Paul, Effects of xanomeline, a selective muscarinic receptor agonist, on cognitive function and behavioral symptoms in Alzheimer disease. *Arch. Neurol.* **54**, 465–473 (1997).
5. A. E. Veroff, N. C. Bodick, W. W. Offen, J. J. Sramek, N. R. Cutler, Efficacy of Xanomeline in Alzheimer disease: Cognitive improvement measured using the computerized neuropsychological test battery (CNTB). *Alzheimer Dis. Assoc. Disord.* **12**, 304–312 (1998).
6. C. C. Felder, P. J. Goldsmith, K. Jackson, H. E. Sanger, D. A. Evans, A. J. Mogg, L. M. Broad, Current status of muscarinic M1 and M4 receptors as drug targets for neurodegenerative diseases. *Neuropharmacology* **136**, 449–458 (2018).
7. E. T. Tzavara, F. P. Bymaster, R. J. Davis, M. R. Wade, K. W. Perry, J. Wess, D. L. McKinzie, C. Felder, G. G. Nomikos, M4 muscarinic receptors regulate the dynamics of cholinergic and dopaminergic neurotransmission: Relevance to the pathophysiology and treatment of related CNS pathologies. *FASEB J.* **18**, 1410–1412 (2004).
8. E. P. Lebois, C. Thorn, J. R. Edgerton, M. Popiolek, S. Xi, Muscarinic receptor subtype distribution in the central nervous system and relevance to aging and Alzheimer's disease. *Neuropharmacology* **136**, 362–373 (2018).
9. C. A. Thorn, J. Moon, C. A. Bourbonais, J. Harms, J. R. Edgerton, E. Stark, S. J. Steyn, C. R. Butter, J. T. Lazzaro, R. E. O'Connor, M. Popiolek, Striatal, hippocampal, and cortical networks are differentially responsive to the M4- and M1-muscarinic acetylcholine receptor mediated effects of xanomeline. *ACS Chem. Neurosci.* **10**, 1753–1764 (2019).
10. T. Pancani, C. Bolarinwa, Y. Smith, C. W. Lindsley, P. J. Conn, Z. Xiang, M4 mAChR-mediated modulation of glutamatergic transmission at corticostriatal synapses. *ACS Chem. Neurosci.* **5**, 318–324 (2014).
11. M. Bubser, T. M. Bridges, D. Dencker, R. W. Gould, M. Grannan, M. J. Noetzel, A. Lamsal, C. M. Niswender, J. S. Daniels, M. S. Poslusney, B. J. Melancon, J. C. Tarr, F. W. Byers, J. Wess, M. E. Duggan, J. Dunlop, M. W. Wood, N. J. Brandon, M. R. Wood, C. W. Lindsley, P. J. Conn, C. K. Jones, Selective activation of M4 muscarinic acetylcholine receptors reverses MK-801-induced behavioral impairments and enhances associative learning in rodents. *ACS Chem. Neurosci.* **5**, 920–942 (2014).
12. R. W. Gould, M. D. Grannan, B. W. Gunter, J. Ball, M. Bubser, T. M. Bridges, J. Wess, M. W. Wood, N. J. Brandon, M. E. Duggan, C. M. Niswender, C. W. Lindsley, P. J. Conn, C. K. Jones, Cognitive enhancement and antipsychotic-like activity following repeated dosing with the selective M4 PAM VU0467154. *Neuropharmacology* **128**, 492–502 (2018).
13. F. P. Bymaster, P. A. Carter, M. Yamada, J. Gomez, J. Wess, S. E. Hamilton, N. M. Nathanson, D. L. McKinzie, C. C. Felder, Role of specific muscarinic receptor subtypes in cholinergic parasympathomimetic responses, in vivo phosphoinositide hydrolysis, and pilocarpine-induced seizure activity. *Eur. J. Neurosci.* **17**, 1403–1410 (2003).
14. A. Christopoulos, Allosteric binding sites on cell-surface receptors: Novel targets for drug discovery. *Nat. Rev. Drug Discov.* **1**, 198–210 (2002).
15. A. Bock, R. Schrage, K. Mohr, Allosteric modulators targeting CNS muscarinic receptors. *Neuropharmacology* **136**, 427–437 (2018).
16. P. Morgan, P. H. Van Der Graaf, J. Arrowsmith, D. E. Feltner, K. S. Drummond, C. D. Wegner, S. D. A. Street, Can the flow of medicines be improved? Fundamental pharmacokinetic and pharmacological principles toward improving phase II survival. *Drug Discov. Today* **17**, 419–424 (2012).
17. R. J. Hargreaves, E. A. Rabiner, Translational PET imaging research. *Neurobiol. Dis.* **61**, 32–38 (2014).
18. H. Hampel, M.-M. Mesulam, A. C. Cuello, M. R. Farlow, E. Giacobini, G. T. Grossberg, A. S. Khachaturian, A. Vergallo, E. Cavedo, P. J. Snyder, Z. S. Khachaturian, The cholinergic system in the pathophysiology and treatment of Alzheimer's disease. *Brain* **141**, 1917–1933 (2018).

19. D. D. Flynn, G. Ferrari-DiLeo, A. I. Levey, D. C. Mash, Differential alterations in muscarinic receptor subtypes in Alzheimer's disease: Implications for cholinergic-based therapies. *Life Sci.* **56**, 869–876 (1995).
20. E. Scarr, C. McLean, B. Dean, Higher levels of different muscarinic receptors in the cortex and hippocampus from subjects with Alzheimer's disease. *J. Neural Transm.* **124**, 273–284 (2017).
21. S. Z. Wang, S. Z. Zhu, D. C. Mash, E. E. el-Fakahany, Comparison of the concentration of messenger RNA encoding four muscarinic receptor subtypes in control and Alzheimer brains. *Brain Res. Mol. Brain Res.* **16**, 64–70 (1992).
22. D. J. Foster, P. J. Conn, Allosteric modulation of GPCRs: New insights and potential utility for treatment of schizophrenia and other CNS disorders. *Neuron* **94**, 431–446 (2017).
23. S. J. Colloby, I. G. McKeith, D. J. Wyper, J. T. O'Brien, J.-P. Taylor, Regional covariance of muscarinic acetylcholine receptors in Alzheimer's disease using (R, R) [¹²³I]-QNB SPECT. *J. Neurool.* **262**, 2144–2153 (2015).
24. S. Shimohama, T. Taniguchi, M. Fujiwara, M. Kameyama, Changes in nicotinic and muscarinic cholinergic receptors in Alzheimer-type dementia. *J. Neurochem.* **46**, 288–293 (1986).
25. L. Tong, W. Li, M. M.-C. Lo, X. Gao, J. M.-C. Wai, M. Rudd, D. Tellers, A. Joshi, Z. Zeng, P. Miller, C. Salinas, K. Riffel, H. Haley, M. Purcell, M. Holahan, L. Gantert, J. W. Schubert, K. Jones, J. Mulhearn, M. Egbertson, Z. Meng, B. Hanney, R. Gomez, S. T. Harrison, P. McQuade, T. Bueters, J. Uslaner, J. Morrow, F. Thomson, J. Kong, J. Liao, O. Selyutin, J. Bao, N. B. Hastings, S. Agrawal, B. C. Magliaro, F. J. Monsma Jr., M. D. Smith, S. Risso, D. Hesk, E. Hostetler, R. Mazzola, Discovery of [¹¹C]MK-6884: A positron emission tomography (PET) imaging agent for the study of M4Muscarinic receptor positive allosteric modulators (PAMs) in neurodegenerative diseases. *J. Med. Chem.* **63**, 2411–2425 (2020).
26. R. Mazzola, S. Lee, M. Lo, L. Tong, X. Gao, R. Ferguson, D. Ondeyka, J. Acton, O. Selyutin, Y. Yu, J. Bao, A. Stamford, W. Li, N. Hastings, F. Monsma, S. Grauer, G. Varty, M. Smith, S. Agrawal, A. Gilotti, K. Feng, J. Kong, E. R. Hostetler, P. Rearden, T. Bueters, J. Uslaner, A. Struyk, A. Basile, S. Smith, F. Thompson, J. Morrow, Discovery of MK-4710: A potent, selective, and bioavailable M4 positive allosteric modulator (PAM), in *Fall ACS Virtual Meeting & Expo*, United States, 17 to 20 August 2020.
27. J. D. Vardigan, C. E. Cannon, V. Puri, M. Dancho, A. Koser, M. Wittmann, S. D. Kuduk, J. J. Renger, J. M. Uslaner, Improved cognition without adverse effects: Novel M1 muscarinic potentiator compares favorably to donepezil and xanomeline in rhesus monkey. *Psychopharmacology* **232**, 1859–1866 (2015).
28. T. Kosasa, Y. Kuriya, K. Matsui, Y. Yamanishi, Effect of donepezil hydrochloride (E2020) on basal concentration of extracellular acetylcholine in the hippocampus of rats. *Eur. J. Pharmacol.* **380**, 101–107 (1999).
29. K. H. Haug, I. L. Bogen, H. Osmundsen, I. Walaas, F. Fonnum, Effects on cholinergic markers in rat brain and blood after short and prolonged administration of donepezil. *Neurochem. Res.* **30**, 1511–1520 (2005).
30. W. Y. Chan, D. L. McKinzie, S. Bose, S. N. Mitchell, J. M. Witkin, R. C. Thompson, A. Christopoulos, S. Lazareno, N. J. M. Birdsall, F. P. Bymaster, C. C. Felder, Allosteric modulation of the muscarinic M4 receptor as an approach to treating schizophrenia. *Proc. Natl. Acad. Sci. U.S.A.* **105**, 10978–10983 (2008).
31. S. P. Moran, J. Maksymetz, P. J. Conn, Targeting muscarinic acetylcholine receptors for the treatment of psychiatric and neurological disorders. *Trends Pharmacol. Sci.* **40**, 1006–1020 (2019).
32. J. P. Bolam, B. H. Wainer, A. D. Smith, Characterization of cholinergic neurons in the rat neostriatum. A combination of choline acetyltransferase immunocytochemistry, Golgi-impregnation and electron microscopy. *Neuroscience* **12**, 711–718 (1984).
33. C. Contant, D. Umbriaco, S. Garcia, K. C. Watkins, L. Descarries, Ultrastructural characterization of the acetylcholine innervation in adult rat neostriatum. *Neuroscience* **71**, 937–947 (1996).
34. A. G. Nair, L. R. V. Castro, M. El Khoury, V. Gorgievski, B. Giros, E. T. Tzavara, J. Hellgren-Kotaleski, P. Vincent, The high efficacy of muscarinic M4 receptor in D1 medium spiny neurons reverses striatal hyperdopaminergia. *Neuropharmacology* **146**, 74–83 (2019).
35. L. S. Kegeles, A. Abi-Dargham, W. G. Frankle, R. Gil, T. B. Cooper, M. Slifstein, D.-R. Hwang, Y. Huang, S. N. Haber, M. Laruelle, Increased synaptic dopamine function in associative regions of the striatum in schizophrenia. *Arch. Gen. Psychiatry* **67**, 231–239 (2010).
36. R. A. McCutcheon, A. Abi-Dargham, O. D. Howes, Schizophrenia, dopamine and the striatum: From biology to symptoms. *Trends Neurosci.* **42**, 205–220 (2019).
37. D. B. Lester, T. D. Rogers, C. D. Blaha, Acetylcholine-dopamine interactions in the pathophysiology and treatment of CNS disorders. *CNS Neurosci. Ther.* **16**, 137–162 (2010).
38. M. M. Mesulam, Cholinergic circuitry of the human nucleus basalis and its fate in Alzheimer's disease. *J. Comp. Neurol.* **521**, 4124–4144 (2013).
39. O. L. Lopez, J. T. Becker, S. Wisniewski, J. Saxton, D. I. Kaufer, S. T. DeKosky, Cholinesterase inhibitor treatment alters the natural history of Alzheimer's disease. *J. Neurol. Neurosurg. Psychiatry* **72**, 310–314 (2002).
40. M.-K. Chen, A. P. Mecca, M. Naganawa, S. J. Finnema, T. Toyonaga, S.-F. Lin, S. Najafzadeh, J. Ropchan, Y. Lu, J. W. McDonald, H. R. Michalak, N. B. Nabulsi, A. F. T. Arnsten, Y. Huang, R. E. Carson, C. H. van Dyck, Assessing synaptic density in Alzheimer disease with synaptic vesicle glycoprotein 2A positron emission tomographic imaging. *JAMA Neurol.* **75**, 1215–1224 (2018).
41. C. Bastin, M. A. Bahri, F. Meyer, M. Manard, E. Delhaye, A. Plenevaux, G. Becker, A. Seret, C. Mella, F. Giacomelli, C. Degueldre, E. Balteau, A. Luxen, E. Salmon, In vivo imaging of synaptic loss in Alzheimer's disease with [¹⁸F]JUCB-H positron emission tomography. *Eur. J. Nucl. Med. Mol. Imaging* **47**, 390–402 (2020).
42. M. Groleau, J. I. Kang, F. Huppé-Gourguet, E. Vaucher, Distribution and effects of the muscarinic receptor subtypes in the primary visual cortex. *Front. Synaptic Neurosci.* **7**, 10 (2015).
43. S. Soma, S. Shimegi, H. Osaki, H. Sato, Cholinergic modulation of response gain in the primary visual cortex of the macaque. *J. Neurophysiol.* **107**, 283–291 (2012).
44. Q. Gu, Contribution of acetylcholine to visual cortex plasticity. *Neurobiol. Learn. Mem.* **80**, 291–301 (2003).
45. T. Iachini, A. Iavarone, V. P. Senese, F. Ruotolo, G. Ruggiero, Visuospatial memory in healthy elderly, AD and MCI: A review. *Curr. Aging Sci.* **2**, 43–59 (2009).
46. T. G. Hamill, N. Sato, M. Jitsuoka, S. Tokita, S. Sanabria, W. Eng, C. Ryan, S. Krause, N. Takenaga, S. Patel, Z. Zeng, D. W. Jr, C. Sur, R. Hargreaves, H. D. Burns, Histamine H3 inverse agonist pet tracers labelled with carbon-11 or fluorine-18. *Neuroimage* **41**, T22 (2008).
47. P. J. Tiseo, S. L. Rogers, L. T. Friedhoff, Pharmacokinetic and pharmacodynamic profile of donepezil HCl following evening administration. *Brit. J. Clin. Pharmacol.* **46**, 13–18 (1998).
48. T. Ota, H. Shinotoh, K. Fukushi, T. Kikuchi, K. Sato, N. Tanaka, H. Shimada, S. Hirano, M. Miyoshi, H. Arai, T. Suhara, T. Irie, Estimation of plasma IC50 of donepezil for cerebral acetylcholinesterase inhibition in patients with Alzheimer disease using positron emission tomography. *Clin. Neuropharmacol.* **33**, 74–78 (2010).

Acknowledgments: We would like to thank the MRL, WP veterinarian associates S. Jendrowski, T. Montgomery, W. Watson, and L. Carangia for help with instrumenting and monitoring the microneurography animals and for assistance with dosing and blood draws. We thank the patients, their caregivers, and other participants for their engagement in this study. **Funding:** W.L., Y.W., T.G.L., Z.Z., L.T., R.M., K.R., P.M., M.P., M.H., H.H., L.G., D.H., S.R., J.M., J.U., A.S., J.M.-C.W., M.T.R., D.M.T., T.M., R.D., I.D.L., A.C., A.H., T.B., M.S.A., E.D.H., and A.S.B. are employed by Merck Sharp & Dohme Corp., a subsidiary of Merck & Co. Inc., Kenilworth, NJ, USA. G.B., M.K., K.V.L., K.S., and J.d.H. are employed by the KU Leuven and Univ Hospital, Leuven, Belgium. M.B.P., P.Z.-F., M.Y., V.A., and J.C.M. are employees of Houston Methodist Neurological Institute, Houston, TX, USA. **Author contributions:** Study conceptualization: W.L., Y.W., T.G.L., Z.Z., L.T., J.M., J.U., A.S., G.B., K.V.L., J.C.M., T.B., M.S.A., E.D.H., and A.S.B. PET tracer discovery and characterization: W.L., Z.Z., L.T., R.M., K.R., P.M., M.P., M.H., H.H., L.G., J.M., J.U., A.S., J.M.-C.W., M.T.R., D.M.T., T.B., and E.D.H. Clinical data acquisition, processing, and quality control: W.L., Y.W., T.G.L., T.M., G.B., M.K., K.S., K.V.L., J.d.H., R.D., I.D.L., M.B.P., J.C.M., P.Z.-F., M.Y., V.A., J.C.M., A.C., A.H., T.B., M.S.A., E.D.H., and A.S.B. Manuscript drafting and revising: W.L., Y.W., Z.Z., J.M., J.U., D.H., G.B., K.V.L., J.d.H., R.D., I.D.L., J.C.M., T.B., A.H., E.D.H., and A.S.B. **Competing interests:** W.L., Z.Z., L.T., R.M., J.M., J.U., M.T.R., A.S., A.C., A.H., T.B., M.S.A., E.D.H., and A.S.B. own shares of Merck & Co. Inc. stock. All other authors declare that they have no competing interests. M.T.R., D.M.T., and J.M.-C.W. are inventors on issued U.S. patents US10512638B2 and US10933053B2 and applications WO2017107089 and WO2017112556 held by Merck Sharp & Dohme Corp./MSD. L.T. and R.M. are inventors on issued U.S. patent US10933053B2 and applications WO2017107089 and WO2017112556 held by Merck Sharp & Dohme Corp./MSD. **Data and materials availability:** All data associated with this study are present in the paper or the Supplementary Materials. Requests for MK-6884 precursor and reference standard may be considered based on availability of supply and through Enigma Biomedical Group (license agreement with Merck for novel MK-6884 imaging agent).

Submitted 31 December 2020

Accepted 13 November 2021

Published 12 January 2022

10.1126/scitranslmed.abg3684

The PET tracer [C]MK-6884 quantifies M4 muscarinic receptor in rhesus monkeys and patients with Alzheimer's disease

Wenping LiYuchuan WangTalakat G. LohithZhizhen ZengLing TongRobert MazzolaKerry RiffelPatricia MillerMona PurcellMarie HolahanHyking HaleyLiza GantertDavid HeskSumei RenJohn MorrowJason UslanerArie StruykJenny Miu-Chun WaiMichael T. RuddDavid M. TellersThomas McAvoyGuy BormansMichel KooleKoen Van LaereKim SerdonsJan de HoonRuben DeclercqInge De LepeleireMaria B. PascualPaolo Zanotti-FregonaraMeixiang YuVictoria ArbonesJoseph C. MasdeuAmy ChengAzher HussainTjerk BuetersMatt S. AndersonEric D. HostetlerAnthony S. Basile

Sci. Transl. Med., 14 (627), eabg3684. • DOI: 10.1126/scitranslmed.abg3684

Quantifying M4R engagement

Activation of the M4 muscarinic receptor (M4R) might be therapeutic in patients with Alzheimer's disease (AD). However, the development of selective agonists is hindered by the lack of *in vivo* methods to measure target engagement. Now, Li *et al.* developed a positron emission tomography (PET) tracer called [C]MK-6884 able to bind an allosteric site of M4R with high selectivity. Characterization of the tracer in monkeys, healthy human volunteers, and patients with AD showed selective target engagement and sensitivity to the orthosteric M4R agonist carbachol *in vitro* and to the acetylcholinesterase inhibitor donepezil *in vivo* in monkeys and healthy human volunteers. The results suggest that [C]MK-6884 could be used to measure target engagement in clinical trials and drug development.

View the article online

<https://www.science.org/doi/10.1126/scitranslmed.abg3684>

Permissions

<https://www.science.org/help/reprints-and-permissions>

Use of think article is subject to the [Terms of service](#)

Science Translational Medicine (ISSN) is published by the American Association for the Advancement of Science. 1200 New York Avenue NW, Washington, DC 20005. The title *Science Translational Medicine* is a registered trademark of AAAS. Copyright © 2022 The Authors, some rights reserved; exclusive licensee American Association for the Advancement of Science. No claim to original U.S. Government Works